Realization of non-$\mathcal{PT}$-symmetric optical potentials with all-real spectra in a coherent atomic system

Chao Hang,[1,2,*] Gregory Gabadadze,[2,3,†] and Guoxiang Huang[1,2,‡]

[1]*State Key Laboratory of Precision Spectroscopy, East China Normal University, Shanghai 200062, China*

[2]*NYU-ECNU Joint Institute of Physics at NYU-Shanghai, Shanghai 200062, China*

[3]*Department of Physics, New York University, New York, New York 10003, USA*

(Received 17 November 2016; published 21 February 2017)

We present a physical setup for realizing all-real-spectrum optical potentials with arbitrary gain-and-loss distributions in a coherent medium consisting of a cold three-level atomic gas driven by control and probe laser fields. We show that by the interference of Raman resonances and the Stark shift induced by a far-detuned laser field, tunable, non-parity-time (non-$\mathcal{PT}$)-symmetric optical potentials with all-real spectra proposed recently by Nixon and Yang [Phys. Rev. A **93**, 031802(R) (2016)] can be actualized physically. We also show that when the real parts of the non-$\mathcal{PT}$-symmetric optical potentials are tuned cross certain thresholds, phase transitions—where the eigenspectrum of the system changes from all real to complex—may occur and hence the stability of the probe-field propagation is altered. Our scheme can also be extended to high dimensions and to a nonlinear propagation regime, where stable optical solitons with power of the order of nano-Watts may be generated in the system.

DOI: 10.1103/PhysRevA.95.023833

I. INTRODUCTION

In quantum mechanics, the Hermiticity of the Hamiltonian of a physical system, $\hat{H}$, is a sufficient (but not necessary) condition for obtaining a real eigenenergy spectrum; it also ensures the probability conservation (so-called unitary evolution) of the system. Since the pioneering work by Bender [1,2], a wide class of non-Hermitian Hamiltonians has been found to possess entirely real spectra below some threshold of system parameters. The Hamiltonians in that class are said to be parity-time ($\mathcal{PT}$) symmetric, as they obey $[\hat{H}, \hat{P}\hat{T}] = 0$, where $\hat{P}$ and $\hat{T}$ are, respectively, the spatial parity and the time reversal operators. Note that $\hat{P}$ is a linear operator and acts on the wave function ψ of the system as $\hat{P}\psi(\mathbf{r},t) = \psi(-\mathbf{r},t)$, while $\hat{T}$ is not a linear one and acts as $\hat{T}\psi(\mathbf{r},t) = \psi^*(\mathbf{r},-t)$. It then follows that the Hamiltonian with the complex potential $V(\mathbf{r})$ having the $\mathcal{PT}$ symmetry requires the condition $V(\mathbf{r}) = V^*(-\mathbf{r})$, which implies the real (imaginary) part of the potential must be an even (odd) function of position $\mathbf{r}$.

In recent years, a large number of investigations focusing on $\mathcal{PT}$-symmetric Hamiltonians have been conducted at the forefront of research in fundamental physics and applied mathematics (for a recent review, see Ref. [3]). Among these investigations much attention has been paid to the study of $\mathcal{PT}$-symmetric optics, owing to the fact that classical Maxwell equations—under the paraxial approximation describing the propagation properties of light-are mathematically identical to the Schrödinger equation in quantum mechanics. This connection between optics and quantum mechanics not only opens up a new and exciting research territory for non-Hermitian quantum mechanics but also provides an excellent platform for realizing and testing the respective theoretical ideas experimentally, through the manipulation and control of classical light [4–8]. In addition, such investigations have already led to many attractive practical applications, including the realization of nonreciprocal and unidirectional invisible light propagations [9–11], coherent perfect absorbers [12,13], giant light amplification [14], novel lasers [15–17], and so on.

In $\mathcal{PT}$-symmetric optics, the optical potential is represented by the optical refractive index $n(\mathbf{r})$. Optical $\mathcal{PT}$ symmetry requires the real part of the refractive index, Re$[n(\mathbf{r})]$, to be an even function and the imaginary part of the refractive index (i.e., gain-loss distribution), Im$[n(\mathbf{r})]$, to be an odd function in space [18], which is, however, quite restrictive. It will be desirable if one can still obtain an all-real spectrum for an optical potential that violates the requirement of $\mathcal{PT}$ symmetry. Several interesting attempts have been made, and examples where complex potentials are not $\mathcal{PT}$ symmetric but with real spectra have been reported [19–21], which stimulated a flush of research activities on non-$\mathcal{PT}$-symmetric systems with real spectra [22–28]. We should also mention that in the path of exploring entirely real eigenvalues in non-$\mathcal{PT}$-symmetric systems, a crucial step is the introduction of the concept of pseudo-Hermiticity, first introduced in Ref. [29].

In a recent work, Nixon and Yang [30] proposed a very general mathematical approach for searching a non-$\mathcal{PT}$-symmetric complex potential that allows an all-real spectrum. They suggested several such potentials with gain-loss distribution fairly arbitrary and showed that the non-$\mathcal{PT}$-symmetric potentials they suggested may undergo phase transitions, i.e., the eigenspectra are changed from all-real to complex when system parameters go across some thresholds. It is natural to ask the following question: Is it possible to design a realistic physical system for realizing such non-$\mathcal{PT}$-symmetric potentials?

In this article, we give a positive answer for the above question by presenting a physical setup to realize the non-$\mathcal{PT}$-symmetric optical potentials with all-real spectra. The system we suggest is a coherent medium consisting of a cold three-level atomic gas with two species driven by control and probe laser fields. We show that, by the interference

*chang@phy.ecnu.edu.cn

†gabadadze@physics.nyu.edu

‡gxhuang@phy.ecnu.edu.cn

of Raman resonances and the Stark shift induced by a far-detuned laser field, tunable, non-$\mathcal{PT}$-symmetric optical potentials with all-real spectra proposed recently in Ref. [30] can be actualized physically. We also show that, when the real parts of the non-$\mathcal{PT}$-symmetric optical potentials are tuned across certain thresholds, phase transitions—where the eigenspectrum changes from all-real to complex—may occur and hence the stability of probe field propagation is changed across the thresholds. We further show that our scheme can be extended to high dimensions and to a nonlinear propagation regime, where stable optical solitons with power of the order of nano-Watts can be generated in such a non-$\mathcal{PT}$-symmetric optical system.

Before preceding, we note that $\mathcal{PT}$-symmetric optical potentials have been suggested and realized experimentally in coherent atomic systems with three- and four-level configurations [31–37]. We stress that $\mathcal{PT}$ symmetry based on multilevel atomic gases interacting with laser fields possess many advantages. One of them is that such systems admit authentic optical potentials with $\mathcal{PT}$ symmetry; i.e., the balance between the gain and the loss can be realized in the whole space. In addition, such optical potentials can be easily manipulated and controlled *in situ* with very high precision through the selection of different atomic levels and laser fields and the active adjustment of many system parameters [3]. The research in our work reported below extends the studies in Refs. [3,31–38] to the case of non-$\mathcal{PT}$ symmetry and opens an avenue for the exploration of non-$\mathcal{PT}$-symmetric optics using coherent atomic media, which may have potential applications in optical information processing and transmission, such as the realization of new types of light propagation and the design of novel amplifiers and lasers via non-$\mathcal{PT}$-symmetric optical structures.

The main body of the article is arranged as follows. In Sec. II, we describe our atomic gas model. In Sec. III, we illustrate how to realize non-$\mathcal{PT}$-symmetric optical potentials with all-real spectra by selecting suitable control and Stark laser fields, and we explore the character of light propagation in the system. In Sec. IV, we extend our scheme to high dimensions and a nonlinear propagation regime. The last section contains the summary of the main results of the present work.

II. MODEL

The system we consider consists of two species of cold atoms, i.e., the isotopes of ^{87}Rb (species 1) and ^{85}Rb (species 2), where each atom has a Λ-type level configuration, loaded into a two-dimensional (2D) atomic gas cell [31]. A weak, pulsed probe field $\mathbf{E}_p$ (strong, continuous-wave control field $\mathbf{E}_c$), propagating along the z direction with wave number $k_p \equiv 2\pi/\lambda_p$ ($k_c \equiv 2\pi/\lambda_c$) and angular frequency $\omega_p \equiv k_p c$ ($\omega_c \equiv k_c c$), drives the ground state $|g,s\rangle$ ($|a,s\rangle$) to the excited level $|e,s\rangle$ ($s = 1,2$ indicates the species of the atoms). For the mixture of rubidium isotopes we assign $|g,s\rangle = |5S_{1/2}, F = 1\rangle$, $|a,s\rangle = |5S_{1/2}, F = 2\rangle$, and $|e,s\rangle = |5P_{1/2}, F = 0\rangle$ (see Fig. 1). The half Rabi frequency of the probe field (control field) is defined as $\Omega_p = |\mathbf{e}_p \cdot \mathbf{p}_{\rm eg}| E_p/(2\hbar)$ [$\Omega_c = |\mathbf{e}_c \cdot \mathbf{p}_{\rm ea}| E_c/(2\hbar)$], where $\mathbf{p}_{\rm eg}$ ($\mathbf{p}_{\rm ea}$) are the electric-dipole matrix elements associated with the transition $|e,s\rangle \leftrightarrow |g,s\rangle$ ($|e,s\rangle \leftrightarrow |a,s\rangle$) and are assumed to be approximately equal for both isotopes. For the selected levels of rubidium atoms, $p_{\rm eg} \approx p_{\rm ea} = 2.54 \times 10^{-27}$ C cm [39]. The polarization unit vector and the envelope of the probe field (control field) $\mathbf{e}_p$ and E_p ($\mathbf{e}_c$ and E_c) are, respectively.

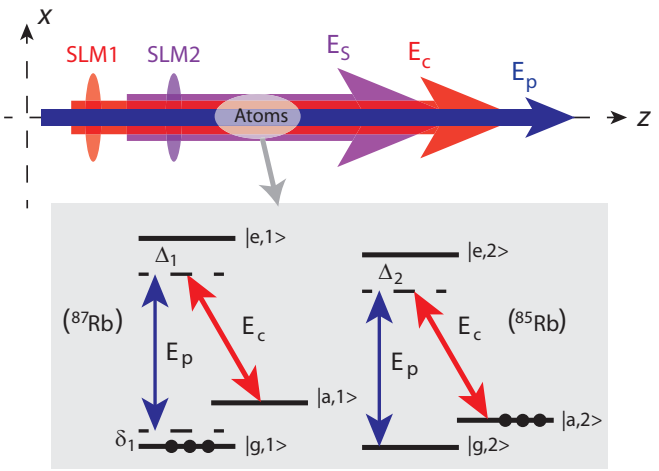

FIG. 1. Energy-level diagram and Raman excitation scheme of the mixed two species of ^{87}Rb and ^{85}Rb atoms with Λ-type configuration of three levels ($|g,s\rangle$, $|a,s\rangle$, $|e,s\rangle$; $s = 1,2$) interacting with the probe field E_p, the control field E_c, and the Stark field E_S. Δ_s ($s = 1,2$) and δ_1 are one- and two-photon detunings, respectively. The black points indicate the energy levels initially populated. SLM1 and SLM2 are spatial light modulators used to produce the spatial distributions of E_c and E_S for acquiring non-$\mathcal{PT}$-symmetric optical refractive indexes of the probe field.

The motions of the atoms and the probe field are governed, respectively, by the optical Bloch equation and the Maxwell equation, which are listed in the Appendix [i.e., Eqs. (A2)–(A8) in the Appendix]. We assume that the time duration of the probe field is large enough that the Maxwell-Bloch (MB) equations can be solved under steady-state approximation. The probe-field susceptibility inside the atomic cell in the steady state is defined by $\chi_p = p_{eg}^2(N_1\rho_{eg}^1 + N_2\rho_{eg}^2)/(\epsilon_0\hbar\Omega_p)$, where N_s is the density of the sth isotope and ρ_{eg}^s is the atomic coherence of the sth isotope ($s = 1,2$). Using the smallness of the amplitude of the probe field, i.e., $|\Omega_p/\Omega_c| \ll 1$, we can employ the expansion $\rho_{jk}^s = \sum_{m=0} \rho_{jk,m}^s$ ($j,k = g,a,e$), where $\rho_{jk,m}^s$ is of the order of magnitude of $|\Omega_p/\Omega_c|^m$. Substituting the expansion into the Bloch equations, Eqs. (A2)–(A8), and neglecting the terms with the time derivative $\partial/\partial t$ (i.e., steady-state approximation), we obtain in the leading order ($m = 0$) the solution $\rho_{gg,0}^1 = \rho_{aa,0}^2 = 1$ and $\rho_{ea,0}^2 = -\Omega_c/d_{ea}^2$, with other matrix elements being zero. The atomic coherence ρ_{eg}^s can be computed from Eqs. (A2)–(A8) in the first order ($m = 1$). We obtain $\rho_{eg,1}^1 = \delta_1\Omega_p/[\delta_1(\delta_1 + \Delta_1 - i\Gamma) - |\Omega_c|^2]$ and $\rho_{eg,1}^2 = \Omega_p/(\Delta_2 + i\Gamma)$, and hence the probe-field susceptibility inside the atomic cell can be expressed as

$$\chi_p = \frac{p_{eg}^2}{\epsilon_0\hbar}(N_1 D_1 + N_2 D_2), \tag{1}$$

with $D_1 \equiv \delta_1/[\delta_1(\delta_1 + \Delta_1 - i\Gamma) - |\Omega_c|^2]$ and $D_2 \equiv 1/(\Delta_2 + i\Gamma)$. Here $\Delta_s \equiv \omega_e^s - \omega_a^s - \omega_c$ and $\delta_s \equiv \omega_a^s - \omega_g^s - (\omega_p - \omega_c)$

are, respectively, one- and two-photon detunings, with $\delta_2 \approx 0$ and $\hbar\omega_a^s$ ($\hbar\omega_g^s$) being the eigenenergy of the level $|a,s\rangle$ ($|g,s\rangle$). In addition, $\Gamma = \Gamma_{eg} \approx \Gamma_{ea}$ with Γ_{eg} (Γ_{ea}) denoting the spontaneous-emission decay rate from $|e,s\rangle$ to $|g,s\rangle$ (from $|e,s\rangle$ to $|a,s\rangle$). The spontaneous-emission decay rate from $|a,s\rangle$ to $|g,s\rangle$ is much smaller than Γ and hence can be neglected, i.e., $\Gamma_{ag} \approx 0$. For a cold and dilute rubidium gas $\Gamma \approx \pi \times 5.75$ MHz, and dephasing processes play a negligible role [39].

In order to acquire a non-$\mathcal{PT}$-symmetric optical potential, a desired spatial distribution of the probe-field susceptibility, and hence of the refractive index $n \approx \sqrt{1+\chi_p}$), is needed. To this end, we assume that an x-dependent, far-detuned laser field (i.e., Stark field), $E_S(x)\cos(\omega_S t)$, is applied to the system, which will induce energy shifts $\Delta E_{j,S}(x) = -\alpha_j E_S^2(x)/4$ for levels $|j,s\rangle$, with α_j being the scalar polarizabilities ($j = g,a,e$). In addition, the control field is also assumed to be x dependent, i.e., $\Omega_c = \Omega_c(x)$. For the selected levels of rubidium atoms stated above, we have $\alpha_e - \alpha_g \approx 2\pi\hbar \times 0.1223$ Hz(cm/V)^2 and $\alpha_g \approx \alpha_a$ [39], and thus $\Delta_s(x) = \Delta_s - (\alpha_e - \alpha_g)E_S^2(x)/(4\hbar)$ and δ_1 is x independent. Note that the characteristic spatial scale of $\Delta_s(x)$ is comparable to the Stark-field wavelength λ_S.

With the probe-field susceptibility obtained above, the equation of motion for the probe-field Rabi frequency given by Eq. (A8) in Appendix is simplified into the form

$$i\frac{\partial q}{\partial \zeta} + \frac{\partial^2 q}{\partial \xi^2} + V(\xi)q = 0, \tag{2}$$

where $q = \Omega_p/\Omega_0$ is the dimensionless Rabi frequency (with Ω_0 being the typical Rabi frequency) of the probe field, and $\zeta = z/(2k_p l_0^2)$ and $\xi = x/l_0$ (with l_0 being a characteristic length comparable to λ_S) are, respectively, dimensionless spatial coordinates along the z and x directions. The second term on the left-hand side of Eq. (2) describes the diffraction of the probe beam. The optical potential $V(\xi)$ in the above equation is given by $V(\xi) = k_p^2 l_0^2 \chi_p(\xi)$, i.e., proportional to the susceptibility of the probe field. Eigenmodes of Eq. (2) have the from $q = \psi(\xi)\exp(i\mu\zeta)$, where ψ satisfies the eigenvalue equation $\hat{L}\psi = \mu\psi$, with $\hat{L} = \partial^2/\partial\xi^2 + V(\xi)$ and μ being the eigenvalue. If we write the potential with the form $V(\xi) = F(\xi) - iG(\xi)$, then the real part $F(\xi)$ reflects the refraction property and the imaginary part $G(\xi)$ represents the gain and loss of the probe field ($G > 0$ corresponds to gain and $G < 0$ corresponds to loss). Note that when deriving Eq. (2) the probe beam has been assumed to have a large spatial width in the y direction so that the diffraction in the y direction can be neglected. Such an assumption is removed in Sec. IV.

III. PHYSICAL REALIZATION OF ALL-REAL-SPECTRUM OPTICAL POTENTIALS WITHOUT $\mathcal{PT}$ SYMMETRY

Recently, Nixon and Yang [30] proposed the following complex potential:

$$V(\xi) = g(\xi)^2 - 2\beta g(\xi) - iG(\xi), \tag{3}$$

for obtaining all-real spectra for the operator $\hat{L}$, where $g(\xi)$ is an arbitrary real function, β is a free real parameter [40], and $G(\xi) = -g'(\xi)$ is the gain-loss distribution function. If $G(\xi)$ is odd [i.e., $G(\xi) = -G(-\xi)$] and $\beta = 0$, then $V(\xi)$ reduces to a $\mathcal{PT}$-symmetric potential. However, because in general cases $G(\xi)$ is arbitrary, $V(\xi)$ can be non-$\mathcal{PT}$ symmetric. Nixon and Yang proved that, by tuning the parameter β, the eigenspectrum of the operator $\hat{L}$ with the non-$\mathcal{PT}$-symmetric potential of the form (3) changes from all-real to partially complex, and hence the system may undergo a phase transition through the adjustment of the "phase transition parameter" β [30].

The main goal of this work is to present a realistic physical scheme to realize non-$\mathcal{PT}$-symmetric optical potentials with the form (3) which have all-real spectra and make the system display phase transitions. To this end, we choose a set of practical parameters of the system, i.e., $\Delta_1 = -9\Gamma$, $\Delta_2 = -8.28\Gamma$, $\delta_1 = 1.81\Gamma$, $l_0 = 15\,\mu$m, and $\lambda_S \approx 8.6\,\mu$m. The electric-dipole matrix element for the given transition of rubidium is $p_{eg} = 2.5377 \times 10^{-27}$ C cm [39]. The atomic densities of the first and second isotopes are chosen as $N_1 \approx 1.0 \times 10^{12}\,\text{cm}^{-3}$ and $N_2 \approx 6.22 \times 10^{11}\,\text{cm}^{-3}$, respectively. Using a method similar to that in Ref. [31], the complex optical potential with the form of (3) can be created by using the control and Stark fields shaped as

$$|\Omega_c(\xi)|^2/\Gamma^2 \approx 0.03[g(\xi) - \beta]^2 + 1.33G(\xi) + C_1, \tag{4}$$

$$E_S(\xi)^2/E_0^2 \approx 0.06[g(\xi) - \beta]^2 - 0.35G(\xi) + C_2, \tag{5}$$

with $C_1 = 6.52 - 0.03\beta^2$, $C_2 = 0.94 - 0.06\beta^2$, $E_0 = 10^4\,\text{V cm}^{-1}$, and β is an arbitrary, real parameter. If the spot size (diameter) is focused onto 100 μm, the Stark field requires laser power of about 9.8 W, which is almost available now by using a quantum cascade laser operating in the midinfrared wavelength range [41]. In addition, the spatial modulations of the control and Stark fields, Eqs. (4) and (5), may be generated by carefully designed, high-resolution spatial light modulators (SLMs). Since all lengths are scaled by l_0, the pixel size of the SLMs should be smaller than 15 μm, which is also available for present-day SLM techniques [42–44].

In addition to the use of SLMs, alternative methods may also be adopted to generate the intended field distributions described above. For instance, by expanding the expressions (4) and (5) in the Fourier series, the main terms in the Fourier series contain only several significant standing-wave components, which can be created by using pairs of counterpropagating laser fields, widely used in the present-day optical experiments [31,38,45].

In order to have a better understanding of the above analysis, in the following we give two concrete examples for realizing the non-$\mathcal{PT}$-symmetric potential (3) and demonstrate that phase transitions may occur in our system. As the first example, we take

$$G(\xi) = -a\,\text{sech}^2[a(\xi + d)] + \text{sech}^2(\xi - d), \tag{6}$$

where the first (second) term is gain (loss) distribution function, both of them are localized in space. For this gain-loss distribution, although no local balance exists between the gain and loss, there is a global balance (i.e., $\int_{-\infty}^{\infty} G(\xi)d\xi = 0$, so the total gain equals to the total loss) in the system. The positive real parameter a appearing in the first term of the right-hand side of (6) describes the amplitude and width of the gain profile, while the positive real parameter d in both terms characterizes the distance between the gain profile and the loss profile. With

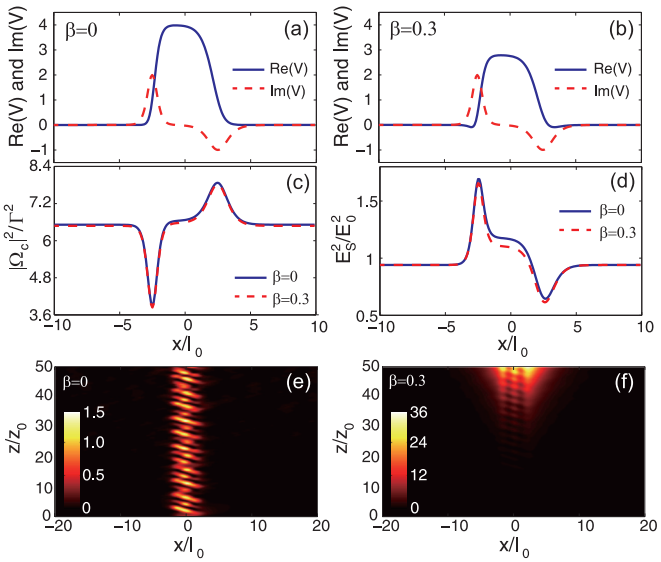

FIG. 2. (a) Real part Re(V) (solid line) and imaginary part Im(V) (dashed line) of V as functions of x/l_0 for $\beta = 0$. (b) The same as panel (a) but with $\beta = 0.3$. (c) and (d) $|\Omega_c|^2/\Gamma^2$ and E_S^2/E_0^2 as functions of x/l_0. The solid (dashed) line corresponds to $\beta = 0$ ($\beta = 0.3$). (e) and (f) Evolutions of probe-field intensity $|\Omega_p|^2/\Omega_0^2$, respectively, for $\beta = 0$ (below the phase transition point, where wave propagation is stable) and for $\beta = 0.3$ (above the phase transition point, where wave propagation is unstable). The initial condition is chosen as $\Omega_p = \Omega_0 e^{-\xi^2}$ in both panels. In all panels, $G(\xi)$ and $g(\xi)$ are, respectively, given by (6) and (7), and the potential parameters are chosen as $a = 2$ and $d = 2.5$; i.e., the optical potentials V shown in panels (a) and (b) are non-$\mathcal{PT}$ symmetric.

(6), we have

$$g(\xi) = \sinh[a(\xi + d)]\mathrm{sech}[a(\xi + d)] - \sinh(\xi - d)\mathrm{sech}(\xi - d). \quad (7)$$

If $a = 1$ (a special case), the optical potential (3) with (6) and (7) is $\mathcal{PT}$ symmetric. However, for $a \neq 1$ (general cases) this potential is non-$\mathcal{PT}$ symmetric. Based on the results (4) and (5), the potential (3) together with (6) and (7) can be produced in the coherent atomic system described in the last section by using the control and Stark fields shaped by

$$\begin{aligned}|\Omega_c(\xi)|^2/\Gamma^2 \approx\ & 0.03\{\sinh[a(\xi + d)]\mathrm{sech}[a(\xi + d)] \\ & - \sinh(x - d)\mathrm{sech}(\xi - d) - \beta\}^2 \\ & -1.33\{a\,\mathrm{sech}^2[a(\xi + d)] \\ & -\mathrm{sech}^2(\xi - d)\} + C_1, \end{aligned} \quad (8)$$

$$\begin{aligned}E_S(\xi)^2/E_0^2 \approx\ & 0.06\{\sinh[a(\xi + d)]\mathrm{sech}[a(\xi + d)] \\ & - \sinh(\xi - d)\mathrm{sech}(\xi - d) - \beta\}^2 \\ & +0.35[a\,\mathrm{sech}^2[a(\xi + d)] \\ & -\mathrm{sech}^2(\xi - d)] + C_2. \end{aligned} \quad (9)$$

Shown in Fig. 2(a) is the real part Re(V) (solid line) and the imaginary part Im(V) (dashed line) of the optical potential V as functions of x/l_0 with $\beta = 0$ and $d = 2.5$. The amplitude and width parameter in the gain function [i.e., the first term of (6)] is chosen as $a = 2$, and hence the optical potential V is non-$\mathcal{PT}$ symmetric. Figure 2(b) shows the case for $\beta = 0.3$ with the other parameters being the same as those in Fig. 2(a). In this case V is also non-$\mathcal{PT}$ symmetric. Shown in Figs. 2(c) and 2(d) are $|\Omega_c|^2/\Gamma^2$ and E_S^2/E_0^2 as functions of x/l_0 with $a = 2$ and $d = 2.5$. The solid line is for $\beta = 0$ and the dashed line is for $\beta = 0.3$.

In order to know the feature of the probe field for different potential parameters, a numerical simulation by using the split-step Fourier method [46] is carried out by choosing different β in the non-$\mathcal{PT}$-symmetric potential V by keeping $a = 2$ and $d = 2.5$ fixed. The result shows that, when β is smaller than the critical value $\beta_{\mathrm{cr}} \approx 0.17$, i.e., $\beta < \beta_{cr}$, the eigenvalues μ of the operator $\hat{L}$ are all-real; however, when $\beta > \beta_{\mathrm{cr}}$, the eigenvalue μ becomes complex. Thus, a phase transition of the system occurs at $\beta = \beta_{\mathrm{cr}} \approx 0.17$.

Figure 2(e) shows the propagation feature of the probe-field intensity $|\Omega_p|^2/\Omega_0^2$ as a function of x/l_0 and z/z_0 ($z_0 \equiv 2k_p l_0^2$) for $a = 2$, $d = 2.5$, and $\beta = 0$. The initial condition is chosen as a Gaussian pulse, $\Omega_p(\xi,0) = \Omega_0 e^{-\xi^2}$. We see that the probe field is stable during propagation. The reason is that in this case the phase transition parameter β of the system locates in the region $\beta < \beta_{\mathrm{cr}}$ where the eigenvalues of $\hat{L}$ are all-real. The oscillation of the amplitude along the z direction is due to the non-$\mathcal{PT}$ symmetry of the optical potential. Shown in Fig. 2(f) is the probe-field propagation for $\beta = 0.3$. Because in this situation the system locates in the region $\beta > \beta_{\mathrm{cr}}$ where the eigenvalues of $\hat{L}$ are complex, the probe field is unstable and is amplified as z increases. Consequently, by adjusting the phase transition parameter β, i.e., by adjusting the profiles of control and Stark fields, we can actively control the phase transition of the system and hence the stability of the probe-field propagation.

As the second example, we take the gain-loss distribution function as

$$G(\xi) = -ae^{-a^2(\xi+d)^2} + e^{-(\xi-d)^2}, \quad (10)$$

for which the total gain and the total loss also balance each other. Then, we have

$$g(\xi) = \frac{\sqrt{\pi}}{2}\{\mathrm{erf}[a(\xi + d)] - \mathrm{erf}(\xi - d)\}, \quad (11)$$

where $\mathrm{erf}(x)$ is the error function defined by $\mathrm{erf}(x) = \frac{2}{\sqrt{\pi}}\int_0^x e^{-\tilde{x}^2}d\tilde{x}$. Potential (3) with (10) and (11) is $\mathcal{PT}$ symmetric (non-$\mathcal{PT}$ symmetric) for $a = 1$ ($a \neq 1$). This potential can be created by using the control and Stark fields shaped as

$$\begin{aligned}|\Omega_c(\xi)|^2/\Gamma^2 \approx\ & 0.03\{\mathrm{erf}[a(\xi + d)] - \mathrm{erf}(\xi - d) - \beta\}^2 \\ & - 1.33[ae^{-a^2(\xi+d)^2} - e^{-(\xi-d)^2}] + C_1, \end{aligned} \quad (12)$$

$$\begin{aligned}E_S(\xi)^2/E_0^2 \approx\ & 0.05\{\mathrm{erf}[a(\xi + d)] - \mathrm{erf}(\xi - d) - \beta\}^2 \\ & + 0.35[ae^{-a^2(\xi+d)^2} - e^{-(\xi-d)^2}] + C_2. \end{aligned} \quad (13)$$

In Figs. 3(a) and 3(b), we show the spatial distributions of the real part Re(V) and the imaginary part Im(V) of the optical potential V [with G and g given by (10) and (11)] for $\beta = 0$ and $\beta = 0.2$, respectively. The other potential parameters are also taken to be $a = 2$ and $d = 2.5$. The spatial modulations of

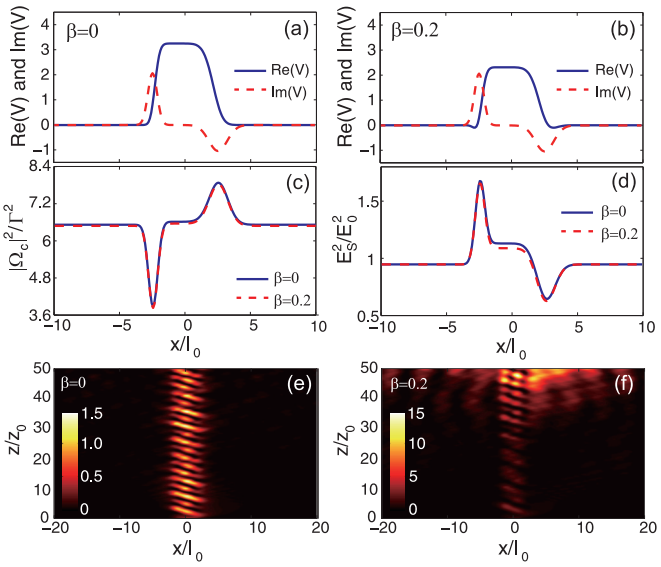

FIG. 3. (a) and (b) Real part Re(V) (solid line) and imaginary part Im(V) (dashed line) of potential (3) as functions of x/l_0 for $\beta = 0$ and $\beta = 0.2$, respectively. (c) and (d) Spatial distributions of $|\Omega_c|^2/\Gamma^2$ and E_S^2/E_0^2, respectively. The solid (dashed) line is for $\beta = 0$ ($\beta = 0.2$). (e) and (f) Evolutions of $|\Omega_p|^2/\Omega_0^2$ for $\beta = 0$ (below the phase transition point, where wave propagation is stable) and $\beta = 0.2$ (above the phase transition point, where wave propagation is unstable), respectively. The initial condition is chosen as $\Omega_p = \Omega_0 e^{-\xi^2}$ for both panels. In all panels, $G(\xi)$ and $g(\xi)$ are, respectively, given by (10) and (11), and the potential parameters are chosen as $a = 2$ and $d = 2.5$; i.e., the optical potentials V shown in panels (a) and (b) are non-$\mathcal{PT}$ symmetric.

$|\Omega_c|^2/\Gamma^2$ and E_S^2/E_0^2 are illustrated, respectively, in Figs. 3(c) and 3(d), where the solid (dashed) line is for $\beta = 0$ ($\beta = 0.2$).

We carried out a numerical simulation for examining the propagation feature of the probe field by using different phase transition parameters β in the non-$\mathcal{PT}$-symmetric potential V with $a = 2$ and $d = 2.5$ being fixed. The result shows that a phase transition indeed occurs in this case, with the critical point of phase transition given by $\beta = \beta_{\rm cr} \approx 0.05$. When $\beta < \beta_{\rm cr}$, the eigenvalues μ of the operator $\hat{L}$ are all-real and the probe-field propagation is stable [see Fig. 3(e) for $\beta = 0$]; when $\beta > \beta_{\rm cr}$, the eigenvalue μ becomes complex and the probe-field propagation is unstable [see Fig. 3(f) for $\beta = 0.2$].

IV. EXTENSION TO HIGH DIMENSIONS AND NONLINEAR REGIME

The above proposal for realizing non-$\mathcal{PT}$-symmetric complex potentials in the coherent atomic gas can be easily extended to higher dimensions. Considering that the atoms are loaded into a 3D atomic cell and the spatial width of the probe beam in the y direction is small so that the diffraction effect in this direction must be taken into account, Eq. (2) must be replaced by

$$i\frac{\partial q}{\partial \zeta} + \frac{\partial^2 q}{\partial \xi^2} + \frac{\partial^2 q}{\partial \eta^2} + V(\xi,\eta)q = 0, \tag{14}$$

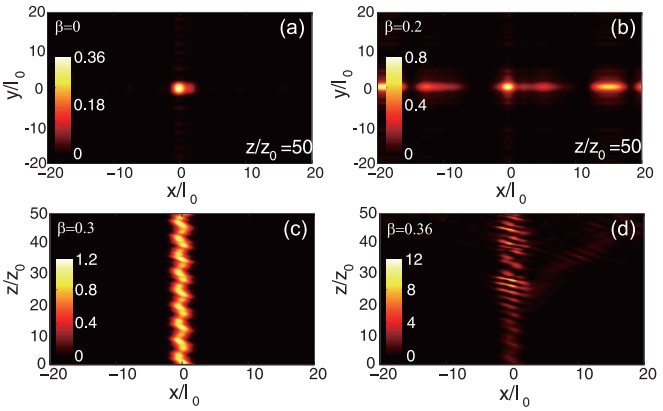

FIG. 4. (a) and (b) Linear evolutions of the probe-field intensity $|\Omega_p|^2/\Omega_0^2$ as functions of x and y at $z/z_0 = 50$ [$G(\xi)$ and $g(\xi)$ are, respectively, taken as (10) and (11) with $a = 2$ and $d = 2.5$] for $\beta = 0$ (below the phase transition point, hence the wave is stable) and $\beta = 0.2$ (above the phase transition point, hence the wave is unstable), respectively. The initial condition is chosen as $\Omega_p = \Omega_0 e^{-\xi^2-\eta^2}$ in both panels. (c) and (d) Nonlinear evolutions of the probe-field intensity $|\Omega_p|^2/\Omega_0^2$. The profiles of $G(\xi)$ and $g(\xi)$ are taken as (10) and (11) but with $\beta = 0.3$ for (c) and $\beta = 0.36$ for (d), respectively. The initial condition is chosen as $\Omega_p = \Omega_0\,\mathrm{sech}(\xi)$ in both panels.

where the 2D complex optical potential has the form

$$V(\xi,\eta) = g^2(\xi) - 2\beta g(\xi) - iG(\xi) + f(\eta), \tag{15}$$

with $\eta = y/l_0$. In the above equation, $f(\eta)$ is a new, arbitrary real function. Since optical potential (15) is separable in the x and y directions, the system allows phase transitions only in the x direction by choosing the spatial distributions of Ω_c and E_S. By means of the phase transitions, one can actively control the stability of the probe beam propagation.

In our atomic system, the 2D complex optical potential (15) can be created by using the control and Stark fields shaped as

$$|\Omega_c(\xi)|^2/\Gamma^2 \approx 0.03[g(\xi) - \beta]^2 + 0.03 f(\eta) + 1.33G(\xi) + C_1, \tag{16}$$

$$E_S(\xi)^2/E_0^2 \approx 0.06[g(\xi) - \beta]^2 + 0.06 f(\eta) - 0.35G(\xi) + C_2, \tag{17}$$

with C_1 and C_2 being the same as those used in Eqs. (4) and (5). Since the 2D complex potential (15) is a linear superposition of the 1D complex potential (3) in the x direction and the 1D real potential $f(\eta)$ in the y direction, the phase transition point for the 2D complex potential (15) is the same as that of the 1D complex potential (3).

As an example, we take $f(\eta) = e^{-\eta^2}$ and $G(\xi)$ and $g(\xi)$ are the same as those given by (10) and (11). Shown in Figs. 4(a) and 4(b) are linear evolutions of the probe-field intensity $|\Omega_p|^2/\Omega_0^2$ as functions of x and y at $z/z_0 = 50$ [$G(\xi)$ and $g(\xi)$ are, respectively, taken as (10) and (11) with $a = 2$ and $d = 2.5$] for $\beta = 0$ (below the phase transition point $\beta_{\rm cr} \approx -0.17$) and $\beta = 0.2$ (above the phase transition point), respectively. The initial condition is chosen as $\Omega_p = \Omega_0 e^{-\xi^2-\eta^2}$ in both panels. We see that, below (above) the phase point, the probe beam is stable (unstable).

Our scheme can also be extended into the nonlinear regime by increasing the intensity of the probe field while keeping it much weaker than that of the control field [3]. The probe-field susceptibility calculated up to the third (i.e., $|\Omega_p/\Omega_c|^3$) order can be written into the form $\chi_p \approx \chi_p^{(1)} + |\Omega_p/\Omega_c|^2\chi_p^{(3)}$, where the first-order (linear) susceptibility is given by Eq. (1), while the third-order (nonlinear) susceptibility reads [38]

$$\chi_p^{(3)} \approx -\frac{p_{eg}^2}{\epsilon_0\hbar}\left\{\frac{N_1}{\Delta_1} + N_1\frac{4|\Omega_c|^2 - 3\delta_1^2 + i\delta\Gamma}{\Delta_1^2\delta} + \frac{3N_2}{\Delta_2} - iN_2\frac{\Gamma}{\Delta_2^2}\right\}. \tag{18}$$

Then, by assuming the diffraction in the y direction can be neglected, we obtain the propagation equation for the probe field:

$$i\frac{\partial q}{\partial\zeta} + \frac{\partial^2 q}{\partial\xi^2} + V(\xi)q + W|q|^2 q = 0, \tag{19}$$

where $W \equiv k_p^2 l_0^2 \frac{\Omega_0^2}{|\Omega_c|^2}\chi_p^{(3)}$ characterizes the Kerr nonlinear effect of the probe field. Due to the resonance character of the system, such a nonlinear effect can be greatly enhanced.

Since Δ_s and Ω_c are chosen to depend on ξ, the third-order susceptibility $\chi_p^{(3)}$ is also space modulated. However, it can be separated by a constant part and a space-modulated part, i.e., $\chi_p^{(3)} = \chi_{p,0}^{(3)} + \chi_{p,1}^{(3)}(\xi)$, since in most regions of the system parameters, the space-modulated part $\chi_{p,1}^{(3)}(\xi)$ is much smaller than the constant part $\chi_{p,0}^{(3)}$ (for the system parameters given in Sec. III, $\chi_{p,1}^{(3)}(\xi)$ is 1 order of magnitude smaller than $\chi_{p,0}^{(3)}$). Consequently, under the required accuracy, the space-modulated part can be safely neglected. In addition, because $\Delta_s \gg \Gamma$, the imaginary part of $\chi_p^{(3)}$ is much smaller than the real part and thus can also be neglected. As a result, $\chi_p^{(3)}$ (and hence W) can be approximated as a real constant. Indeed, with the given parameters we obtain $\chi_p^{(3)} \approx 0.017$, which results in $W \approx 1$ by taking $\Omega_0 \approx 0.2\Gamma$.

Equation (19) supports optical soliton solutions, which may be stable in a wide range of system parameters. Figure 4(c) shows the soliton evolution for the probe-field intensity $|\Omega_p|^2/\Omega_0^2$ by solving Eq. (19) for $W = 1$. The profiles of $G(\xi)$ and $g(\xi)$ are taken as (6) and (7) with $a = 2$, $d = 2.5$, and $\beta = 0.3$, and hence the optical potential $V(\xi)$ is non-$\mathcal{PT}$ symmetric. The initial condition is chosen as $\Omega_p(\xi,0) = \Omega_0\,\mathrm{sech}(\xi)$. From the figure we see that the optical soliton is stable during propagation. Since $\beta(=0.3)$ in this nonlinear case ($W = 1.0$) is larger than the critical value ($\beta_{\rm cr} = 0.17$) of the phase transition in the corresponding linear case ($W = 0$), we deduce that the critical value of the phase transition in the nonlinear case, $\beta_{\rm cr}^{\rm nonl}$, will be larger than that in the linear case (i.e., $\beta_{\rm cr}^{\rm nonl} > \beta_{\rm cr}$).

To check the above deduction and to seek the value of $\beta_{\rm cr}^{\rm nonl}$, we carry out a numerical simulation by examining the propagation character of the optical soliton via changing the value of β. We find $\beta_{\rm cr}^{\rm nonl} \approx 0.32$, i.e., the soliton is stable (unstable) for $\beta < \beta_{\rm cr}^{\rm nonl} = 0.32$ ($\beta > \beta_{\rm cr}^{\rm nonl} = 0.32$). Shown in Fig. 4(d) is the optical soliton evolution for $\beta = 0.36$. We see that the soliton is indeed unstable during propagation because $\beta > \beta_{\rm cr}^{\rm nonl}$. The physical reason for the increase of the critical value of the phase transition in comparison with the linear case is due to the fact that the nonlinear term in Eq. (19) contributes an equivalent potential to the wave function q and hence changes the ratio between the real and imaginary parts of the non-$\mathcal{PT}$-symmetric potential V. Because the nonlinearity in Eq. (19) is of a self-focusing type, it causes a positive shift of the critical value of the phase transition. Note in passing that the nonlinear effect on the phase transition in $\mathcal{PT}$-symmetric systems has been studied recently [47], and the soliton stability in non-$\mathcal{PT}$-symmetric systems has also been explored in Ref. [26].

The power of the optical soliton described in Fig. 4(c) can be estimated by using the Poynting's vector. Taking the beam diameter of the probe field to be the same as 100 μm, we obtain

$$P_{\rm soliton} \approx 3.4\ \mathrm{nW}, \tag{20}$$

which is extremely small compared with the power of solitons in conventional systems such as optical fibers. The reason is that the coherent atomic gas proposed here possesses largely enhanced Kerr nonlinearity due to the resonant feature of the system, Thus, extremely low input power is required for generating the stable optical solitons in the coherent atomic system with the non-$\mathcal{PT}$-symmetric optical potentials suggested above.

V. CONCLUSION

In this work, we have presented a realistic physical setup for realizing all-real-spectrum optical potentials with arbitrary gain-and-loss distributions in a coherent atomic medium. The system we suggested consists of a cold three-level atomic gas with two species driven by control and probe laser fields. We have shown that by the interference of Raman resonances and the Stark shift induced by a far-detuned laser field, tunable, non-$\mathcal{PT}$-symmetric optical potentials with all-real spectra proposed recently by Nixon and Yang [30] can be actualized physically in our system. We have also shown that when real parts of the non-$\mathcal{PT}$-symmetric optical potentials are tuned across certain thresholds, phase transitions may occur and hence the stability of probe field propagation is changed across the thresholds. In addition, we have extended our scheme into high dimensions and to a nonlinear propagation regime and demonstrated that stable optical solitons with power of the order of nano-Watts may be generated in such non-$\mathcal{PT}$-symmetric optical system. The research presented here opens an avenue for the exploration of non-$\mathcal{PT}$-symmetric systems with all-real spectra by using coherent atomic media, and the results reported may have potential applications in optical information processing and transmission, including the realization of new types of light propagation and the design of novel amplifiers and lasers based on the properties of non-$\mathcal{PT}$ symmetry.

ACKNOWLEDGMENTS

C.H. and G.H. thank V. V. Konotop for useful conservations. This work was supported by the National Natural Science Foundation of China (NSFC) under Grants No. 11475063 and No. 11474099, the Program of Introducing Talents of Discipline to Universities under Grant No. B12024, and the

National Basic Research Program of China under Grant No. 2016YFA0302103.

APPENDIX: OPTICAL BLOCH EQUATIONS FOR DENSITY MATRIX

Under electric-dipole and rotating-wave approximations, the Hamiltonian of the system in the interaction picture reads

$$\hat{H}_{\rm int} = \sum_{s=1}^{2}\{\hbar[\delta_s|a,s\rangle\langle a,s| + (\Delta_s+\delta_s)|e,s\rangle\langle e,s|] - \hbar(\Omega_p|e,s\rangle\langle g,s| + \Omega_s|e,s\rangle\langle a,s| + \text{H.c.})\}, \quad \text{(A1)}$$

where Δ_s, δ_s, Ω_p, and Ω_s have been defined in the main text. The motion of atoms is governed by the optical Bloch equation [45]:

$$i\frac{\partial}{\partial t}\rho^s_{gg} = i\Gamma_{eg}\rho^s_{ee} - \Omega_p^*\rho^s_{eg} + \Omega_p\rho^{s*}_{eg}, \quad \text{(A2)}$$

$$i\frac{\partial}{\partial t}\rho^s_{aa} = i\Gamma_{ea}\rho^s_{ee} - \Omega_c^*\rho^s_{ea} + \Omega_c\rho^{s*}_{ea}, \quad \text{(A3)}$$

$$i\frac{\partial}{\partial t}\rho^s_{ee} = -i(\Gamma_{eg}+\Gamma_{ea})\rho^s_{ee} + \Omega_p^*\rho^s_{eg} - \Omega_p\rho^{s*}_{eg} + \Omega_c^*\rho^s_{ea} - \Omega_c\rho^{s*}_{ea}, \quad \text{(A4)}$$

$$i\frac{\partial}{\partial t}\rho^s_{ag} = -d^s_{ag}\rho^s_{ag} + \Omega_p\rho^{s*}_{ea} - \Omega_c^*\rho^s_{eg}, \quad \text{(A5)}$$

$$i\frac{\partial}{\partial t}\rho^s_{eg} = -d^s_{eg}\rho^s_{eg} + \Omega_p\left(\rho^s_{ee}-\rho^s_{gg}\right) - \Omega_c\rho^s_{ag}, \quad \text{(A6)}$$

$$i\frac{\partial}{\partial t}\rho^s_{ea} = -d^s_{ea}\rho^s_{ea} + \Omega_c\left(\rho^s_{ee}-\rho^s_{aa}\right) - \Omega_p\rho^{s*}_{ag}, \quad \text{(A7)}$$

where ρ_{ij} are the atomic density matrix elements, $d^s_{ag} \equiv \delta_{s,1}\delta_1 + i\gamma_{ag}$ ($\delta_{i,j}=1$ for $i=j$; $\delta_{i,j}=0$ for $i\neq j$), $d^s_{ea} \equiv -\Delta_s + i\gamma_{ea}$, and $d^s_{eg} \equiv \delta_{s,1}\delta_1 - \Delta_s + i\gamma_{eg}$, with $\delta_1 \ll \Delta_s$. Note that we are interested in the situation where both the control and the probe laser fields contain a large number of photons and hence can be treated as classical fields, and hence a semiclassical approach can be applied. In addition, we assume that the control field is strong so that it is undepleted (i.e., the control-field Rabi frequency ω_c is a constant) during the evolution of the system.

The equation of motion for the probe-field Rabi frequency Ω_p can be obtained by using the Maxwell equation $\nabla^2\mathbf{E}_p - (1/c^2)\partial^2\mathbf{E}_p/\partial t^2 = [1/(\varepsilon_0 c^2)]\partial^2\mathbf{P}/\partial t^2$, where $\mathbf{P} = \sum_{s=1}^{2} N_s\mathbf{p}_{eg,s}\sigma_{eg,s}e^{i(k_p z-\omega_p t)} + \text{c.c.}$ is the polarization intensity of the probe field. Under paraxial and slowly varying envelope approximations, one can derive the equation of motion for the probe-field Rabi frequency Ω_p:

$$i\left(\frac{\partial}{\partial z}+\frac{1}{c}\frac{\partial}{\partial t}\right)\Omega_p + \frac{c}{2\omega_p}\left(\frac{\partial^2}{\partial x^2}+\frac{\partial^2}{\partial y^2}\right)\Omega_p + \kappa_1\rho^1_{eg} + \kappa_2\rho^2_{eg} = 0, \quad \text{(A8)}$$

where $\kappa_s = N_s\omega_p|\mathbf{p}^s_{eg}|^2/(2\epsilon_0\hbar)$ $(s=1,2)$.

[1] C. M. Bender and S. Boettcher, Real Spectra in Non-Hermitian Hamiltonians Having $\mathcal{PT}$ Symmetry, Phys. Rev. Lett. **80**, 5243 (1998).

[2] C. M. Bender, Making sense of non-Hermitian Hamiltonians, Rep. Prog. Phys. **70**, 947 (2007).

[3] V. V. Konotop, J. Yang, and D. A. Zezyulin, Nonlinear waves in $\mathcal{PT}$-symmetric systems, Rev. Mod. Phys. **88**, 035002 (2016).

[4] A. Guo, G. J. Salamo, D. Duchesne, R. Morandotti, M. Volatier-Ravat, V. Aimez, G. A. Siviloglou, and D. N. Christodoulides, Observation of $\mathcal{PT}$-symmetry breaking in complex optical potentials, Phys. Rev. Lett. **103**, 093902 (2009).

[5] C. E. Rüter, K. G. Makris, R. El-Ganainy, D. N. Christodoulides, M. Segev, and D. Kip, Observation of parity-time symmetry in optics, Nat. Phys. **6**, 192 (2010).

[6] A. Regensburger, C. Bersch, M.-A. Miri, G. Onishchukov, D. N. Christodoulides, and U. Peschel, Parity-time synthetic photonic lattices, Nature (London) **488**, 167 (2012).

[7] B. Peng, Ş. K. Özdemir, F. Lei, F. Monifi, M. Gianfreda, G. L. Long, S. Fan, F. Nori, C. M. Bender, and L. Yang, Parity-time-symmetric whispering-gallery microcavities, Nat. Phys. **10**, 394 (2014).

[8] L. Chang, X. Jiang, S. Hua, C. Yang, J. Wen, L. Jiang, G. Li, G. Wang, and M. Xiao, Parity-time symmetry and variable optical isolation in active-passive-coupled microresonators, Nat. Photonics **8**, 524 (2014).

[9] H. Ramezani, T. Kottos, R. El-Ganainy, and D. N. Christodoulides, Unidirectional nonlinear $\mathcal{PT}$-symmetric optical structures, Phys. Rev. A **82**, 043803 (2010).

[10] L. Feng, M. Ayache, J. Huang, Y.-L. Xu, M.-H. Lu, Y.-F. Chen, Y. Fainman, and A. Scherer, Nonreciprocal light propagation in a silicon photonic circuit, Science **333**, 729 (2011).

[11] Z. Lin, H. Ramezani, T. Eichelkraut, T. Kottos, H. Cao, and D. M. Christodoulides, Unidirectional Invisibility Induced by $\mathcal{PT}$-Symmetric Periodic Structures, Phys. Rev. Lett. **106**, 213901 (2011).

[12] S. Longhi, $\mathcal{PT}$-symmetric laser absorber, Phys. Rev. A **82**, 031801(R) (2010).

[13] Y. D. Chong, L. Ge, and A. D. Stone, $\mathcal{PT}$-Symmetry Breaking and Laser-Absorber Modes in Optical Scattering Systems, Phys. Rev. Lett. **106**, 093902 (2011).

[14] V. V. Konotop, V. S. Shchesnovich, and D. A. Zezyulin, Giant amplification of modes in parity-time symmetric waveguides, Phys. Lett. A **376**, 2750 (2012).

[15] L. Feng, Z. J. Wong, R. Ma, Y. Wang, and X. Zhang, Single-mode laser by parity-time symmetry breaking, Science **346**, 972 (2014).

[16] H. Hodaei, M.-A. Miri, M. Heinrich, D. N. Christodoulides, and M. Khajavikhan, Parity-time-symmetric microring lasers, Science **346**, 975 (2014).

[17] C. Hang, G. Huang, and V. V. Konotop, Tunable spectral singularities: Coherent perfect absorber and laser in an atomic medium, New J. Phys. **18**, 085003 (2016).

[18] K. G. Makris, R. El-Ganainy, D. N. Christodoulides, and Z. H. Musslimani, $\mathcal{PT}$-Symmetric Periodic Optical Potentials, Int. J. Theor. Phys. **50**, 1019 (2011).

[19] F. Cannata, G. Junker, and J. Trost, Schrödinger operators with complex potential but real spectrum, Phys. Lett. A **246**, 219 (1998).
[20] M. A. Miri, M. Heinrich, and D. N. Christodoulides, Supersymmetry-generated complex optical potentials with real spectra, Phys. Rev. A **87**, 043819 (2013).
[21] E. N. Tsoy, I. M. Allayarov, and F. Kh. Abdullaev, Stable localized modes in asymmetric waveguides with gain and loss, Opt. Lett. **39**, 4215 (2014).
[22] V. V. Konotop and D. A. Zezyulin, Families of stationary modes in complex potentials, Opt. Lett. **39**, 5535 (2014).
[23] J. Yang, Symmetry breaking of solitons in one-dimensional parity-time-symmetric optical potentials, Opt. Lett. **39**, 5547 (2014).
[24] S. Nixon and J. Yang, Light propagation in periodically modulated complex waveguides, Phys. Rev. A **91**, 033807 (2015).
[25] J. Yang, Symmetry breaking of solitons in two-dimensional complex potentials, Phys. Rev. E **91**, 023201 (2015).
[26] J. Yang and S. Nixon, Stability of soliton families in nonlinear Schrödinger equations with non-parity-time-symmetric complex potentials, Phys. Lett. A **380**, 3803 (2016).
[27] K. G. Makris, Z. H. Musslimani, D. N. Christodoulides, and S. Rotter, Constant-intensity waves and their modulation instability in non-Hermitian potentials, Nat. Commun. **6**, 7257 (2016).
[28] N. Abt, H. Cartarius, and G. Wunner, Supersymmetric model of a Bose-Einstein condensate in a $\mathcal{PT}$-Symmetric double-delta trap, Int. J. Theor. Phys. **54**, 4054 (2015).
[29] A. Mostafazadeh, Pseudo-Hermiticity versus $\mathcal{PT}$ symmetry: The necessary condition for the reality of the spectrum of a non-Hermitian Hamiltonian, J. Math. Phys. **43**, 205 (2002).
[30] S. Nixon and J. Yang, All-real spectra in optical systems with arbitrary gain-and-loss distributions, Phys. Rev. A **93**, 031802(R) (2016).
[31] C. Hang, G. Huang, and V. V. Konotop, $\mathcal{PT}$ Symmetry with a System of Three-Level Atoms, Phys. Rev. Lett. **110**, 083604 (2013).
[32] H.-j. Li, J.-p. Dou, and G. Huang, $\mathcal{PT}$ symmetry via electromagnetically induced transparency, Opt. Express **21**, 32053 (2013).
[33] J. Sheng, M.-A. Miri, D. N. Christodoulides, and M. Xiao, $\mathcal{PT}$-symmetric optical potentials in a coherent atomic medium, Phys. Rev. A **88**, 041803(R) (2013).
[34] C. Hang, D. A. Zezyulin, V. V. Konotop, and G. Huang, Tunable nonlinear parity-time-symmetric defect modes with an atomic cell, Opt. Lett. **38**, 4033 (2013).
[35] C. Hang, D. A. Zezyulin, G. Huang, V. V. Konotop, and B. A. Malomed, Tunable nonlinear double-core $\mathcal{PT}$ -symmetric waveguides, Opt. Lett. **39**, 5387 (2014).
[36] Z. Zhang, Y. Zhang, J. Sheng, L. Yang, M.-A. Miri, D. N. Christodoulides, B. He, Y. Zhang, and M. Xiao, Observation of Parity-Time Symmetry in Optically Induced Atomic Lattices, Phys. Rev. Lett. **117**, 123601 (2016).
[37] P. Peng, W. Cao, C. Shen, W. Qu, J. Wen, L. Jiang, and Y. Xiao, Anti-parity-time symmetry with flying atoms, Nat. Phys. **12**, 1139 (2016).
[38] C. Hang and G. Huang, Weak-light solitons and their active control in a parity-time-symmetric atomic system, Phys. Rev. A **91**, 043833 (2015).
[39] D. Steck, ^{85}Rb D Line Data, http://steck.us/alkalidata.
[40] Note that the parameter β here is equal to the parameter $-c_0$ used in Ref. [30] in order to make the statements on the phase transition here the same as those in physics.
[41] B. Meng and Q. J. Wang, Broadly tunable single-mode mid-infrared quantum cascade lasers, J. Opt. **17**, 023001 (2015).
[42] V. Arrizón, U. Ruiz, R. Carrada, and L. A. González, Pixelated phase computer holograms for the accurate encoding of scalar complex fields, J. Opt. Soc. Am. A **24**, 3500 (2007).
[43] V. Arrizón, D. Sánchez-de-la-Llave, G. Méndez, and U. Ruiz, Efficient generation of periodic and quasi-periodic non-diffractive optical fields with phase holograms, Opt. Express **19**, 10553 (2011).
[44] Y. Bromberg and H. Cao, Generating Non-Rayleigh Speckles with Tailored Intensity Statistics, Phys. Rev. Lett. **112**, 213904 (2014).
[45] R. W. Boyd, *Nonlinear Optics*, 3rd ed. (Academic, San Diego, 2008).
[46] G. Agrawal, *Nonlinear Fiber Optics*, 5th ed. (Elsevier, Amsterdam, 2003).
[47] Y. Lumer, Y. Plotnik, M. C. Rechtsman, and M. Segev, Nonlinearly Induced $\mathcal{PT}$ Transition in Photonic Systems, Phys. Rev. Lett. **111**, 263901 (2013).